Applied Catalysis B: Environmental 86 (2009) 18–26

Contents lists available at ScienceDirect

Applied Catalysis B: Environmental

journal homepage: www.elsevier.com/locate/apcatb

Catalytic properties of Pd supported on $ZnO/ZnAl_2O_4/Al_2O_3$ mixtures in dimethyl ether autothermal reforming

Marita Nilsson [a,*], Kjell Jansson [b], Peter Jozsa [c], Lars J. Pettersson [a]

[a] KTH – Royal Institute of Technology, School of Chemical Science and Engineering, Department of Chemical Engineering and Technology, SE-100 44 Stockholm, Sweden
[b] Stockholm University, Arrhenius Laboratory, Department of Physical, Inorganic and Structural Chemistry, SE-106 91 Stockholm, Sweden
[c] Volvo Technology Corporation, Chalmers Science Park, SE-412 88 Göteborg, Sweden

ARTICLE INFO

Article history:
Received 28 April 2008
Received in revised form 6 July 2008
Accepted 14 July 2008
Available online 19 July 2008

Keywords:
Hydrogen
Dimethyl ether
Autothermal reforming
Pd catalyst
PdZn alloy

ABSTRACT

The catalytic properties of Pd supported on mixtures of zinc oxide, zinc aluminate, and alumina, prepared from γ-alumina and zinc nitrate, were studied for autothermal reforming (ATR) of dimethyl ether (DME). The performance of the catalysts was tested in a small-scale reactor, using cordierite monoliths as substrate. The catalysts exhibited high activity and generated hydrogen-rich product gases with CO concentrations below 5 vol.% in the temperature range between 350 and 450 °C (at O_2:DME = 0.7, H_2O:DME = 2.5, and GHSV = 15000 h^{-1}). The highest DME conversion was obtained for a catalyst in which the support comprised mainly $ZnAl_2O_4$. Physical mixing of the catalysts with γ-Al_2O_3 resulted in increased DME conversion but a lowering of the CO_2 selectivity.

The catalysts were characterized by CO chemisorption, liquid nitrogen adsorption, temperature-programmed desorption of ammonia, temperature-programmed reduction, transmission electron microscopy, and X-ray diffraction. It was found that decreasing surface area and decreasing number of acid sites, caused by thermal treatment during generation of the supports, did not affect the activity negatively. The high CO_2 selectivity of the catalysts was correlated with PdZn alloy formation.

1. Introduction

Global warming and emissions of hazardous compounds are focus of intensive concern worldwide. The exploitation of fossil resources for use in the transportation sector is directly related to the environmental issues and is pushing the development of alternative solutions. Biomass-derived dimethyl ether (DME) is a possible alternative fuel in society's effort to bridge the gap between today's transportation solution and a more sustainable future. As a compression ignition engine fuel, the efficiency from well to wheels is high [1]. Furthermore, DME is a promising candidate as a hydrogen carrier for fuel cells in auxiliary power units (APUs) onboard heavy-duty vehicles. Hydrogen-rich fuel cell feed gases can be generated through reforming processes at relatively low temperatures (300–500 °C) compared to conventional fuels such as diesel and gasoline. The low reforming temperature is advantageous in that the reformate contains low concentrations of carbon monoxide and could therefore be fed to high-temperature polymer electrolyte fuel cells, operating at 150–200 °C [2], without need for numerous CO cleanup steps downstream the reformer; a low-temperature water-gas shift unit could be sufficient.

The most thermally efficient and dynamic method of producing hydrogen from transportation fuels is autothermal reforming (ATR) also termed oxidative steam reforming (OSR) or combined reforming. Potential reactions involved during DME ATR conditions are shown in Table 1 (reactions leading to carbon formation are not included). In ATR, the fuel is reacted with air and steam, in order to combine the endothermic steam reforming (Reaction (I)) and the exothermic partial oxidation reaction (Reaction (II)). Steam reforming of DME comprises two sequential reactions [3–5]: DME hydrolysis (Reaction (III)) and methanol steam reforming (Reaction (IV)). DME hydrolysis is catalyzed by solid acids [3,6,7] whereas methanol steam reforming typically is performed over Cu or Pd catalysts [8]. Partial oxidation of DME has been studied over various metal catalysts supported on Al_2O_3 and over Ni on different supports [9,10]. For ATR, a catalyst active for both steam reforming and partial oxidation is required. The ATR reactor can be divided in two zones [11], a first one where partial oxidation preferentially occurs and produces heat to sustain the steam reforming reaction, and a second where mainly steam reforming occurs. Further, a DME steam reforming catalyst needs to be active both for DME hydrolysis and for methanol steam reforming. A possible approach is to use a physical mixture of a DME hydrolysis and a methanol

* Corresponding author. Tel.: +46 87909150.
E-mail address: marita@ket.kth.se (M. Nilsson).

0926-3373/$ – see front matter © 2008 Elsevier B.V. All rights reserved.
doi:10.1016/j.apcatb.2008.07.012

Table 1
Main reaction pathways during DME ATR conditions

Reaction	Chemical formula	ΔH_R° [kJ/mol]
DME steam reforming	$CH_3OCH_3 + 3H_2O(g) \rightarrow 2CO_2 + 6H_2$ (I)	+122
DME partial oxidation	$CH_3OCH_3 + 1/2O_2 \rightarrow 2CO + 3H_2$ (II)	−38
DME hydrolysis	$CH_3OCH_3 + H_2O(g) \rightarrow 2CO_3OH(g)$ (III)	+24
MeOH steam reforming	$CH_3OH(g) + H_2O(g) \rightarrow 3H_2 + CO_2$ (IV)	+49
Water-gas shift	$CO + H_2O(g) \rightarrow CO_2 + H_2$ (V)	−41
DME decomposition	$CH_3OCH_3 + H_2 + CO_2 + CH_4$ (VI)	−1
MeOH decomposition	$CH_3OH(g) \rightarrow 2H_2 + CO$ (VII)	+90
DME total oxidation	$CH_3OCH_3 + 3O_2 \rightarrow 2CO_2 + 3H_2O(g)$ (VIII)	−1330

steam reforming catalyst. Cu-based catalysts are commonly used in methanol steam reforming but have the disadvantage of poor thermal stability at temperatures above approximately 300–350 °C [12]. Pd/ZnO catalysts are known to exhibit high selectivity to CO_2 and H_2 during methanol steam reforming [13,14]. This feature is ascribed to strong chemical interactions between Pd and ZnO that leads to the formation of a PdZn alloy (1:1 atomic ratio), which decreases the activity of decomposition reactions that are otherwise favored over Pd metal [15,16]. In a density functional study by Chen et al. [17], it is suggested that the similar catalytic properties of the 1:1 PdZn alloy and Cu is attributable to similarities in their local electronic structures, being different from that of Pd(0).

Previous research by the authors of this paper focused on the evaluation of Pd-based catalysts supported on cordierite monoliths for autothermal reforming of dimethyl ether [18]. PdZn/γ–Al_2O_3 catalysts, prepared by incipient-wetness impregnation, were shown to exhibit high selectivity in DME autothermal reforming, producing mainly hydrogen and carbon dioxide. In the present study, the main objective has been to further improve the PdZn-based DME ATR catalyst in terms of activity and selectivity. $ZnAl_2O_4$ is a very interesting noble metal support, with high thermal and mechanical stability. The presence of $ZnAl_2O_4$ and ZnO on Al_2O_3 has been shown to effectively screen interactions between Pd–Zn alloys and Al_2O_3, thereby preventing the formation of metallic Pd species during oxidative steam reforming of methanol [19]. In this paper, two different catalyst materials have been prepared by impregnating Pd nitrate onto mixtures of oxides (ZnO, $ZnAl_2O_4$ and Al_2O_3), generated via calcination of Zn-impregnated γ-Al_2O_3, followed by reduction treatment. The results from the activity tests were compared to those obtained using a PdZn/γ–Al_2O_3 catalyst. Physical mixtures of the catalysts with γ-Al_2O_3 were also tested for comparison. Various characterization techniques have been employed in order to elucidate the properties of the catalysts.

2. Experimental

2.1. Catalyst preparation

The catalysts were prepared by impregnating γ-Al_2O_3 powder (Sasol GmbH) with an aqueous solution of zinc nitrate (Alfa Aesar), at a Zn:Al ratio of 1:2 mol:mol, using the incipient-wetness technique. This was done in several steps with drying in between. Following drying overnight at 110 °C, the powder was calcined in air for 5 h at 400 °C. From the resulting ZnO/γ-Al_2O_3 powder, three materials were obtained by calcining at different temperatures (400, 700 and 1000 °C, respectively) for 24 h. Each material was then impregnated with a solution of Pd-nitrate (Alfa Aesar) at a Pd:Zn ratio of 1:9 w/w and calcined again at 400 °C for 5 h. The catalysts are henceforth denoted Pd/ZA(400), Pd/ZA(700), and Pd/ZA(1000), where the numbers in parentheses correspond to the calcination temperature of the Zn–Al oxide supports. The compositions of the materials are shown in Table 2.

For the DME ATR activity tests, the catalyst powders were deposited onto cordierite monoliths (20 mm diameter, 35 mm length) with 400 cpsi (62 cells/cm^2). The catalyst powders were suspended in ethanol and ball-milled for 24 h. The monoliths were dipped into the slurries and dried for 2 h at 110 °C. This procedure was repeated until the loading of catalyst washcoat on the monoliths was 20 ± 1 wt%. The coated monoliths were then calcined in air at 400 °C for 5 h. Physical mixtures of the catalysts and γ-Al_2O_3 (Pd/ZA:γ-Al_2O_3 = 2:1 w/w) were prepared by mixing the powders prior to the ball-milling. The physically mixed catalysts are denoted Pd/ZA(700)+γ-Al_2O_3 and Pd/ZA(1000)+γ-Al_2O_3, respectively, and referred to in the text as the alumina mixtures.

Prior to reaction, the catalysts were activated in situ in a stream of 5% H_2 in N_2 at 400 °C and a flowrate of 1000 Ncm^3/min for 1 h.

Table 2
Composition, surface area, CO uptake, and acidic properties of the DME ATR catalysts

	Pd/ZA(400)	Pd/ZA(700)	Pd/ZA(1000)
Phases identified[a]	γ-Al_2O_3, ZnO, PdZn	Al_2O_3, ZnO, $ZnAl_2O_4$, PdZn	$ZnAl_2O_4$, ZnO, Al_2O_3[a′], PdZn
Pd content [wt%][b]	3.8	3.7	3.5
Zn content [wt%][b]	35	36	34
BET surface area [$m^2\ g^{-1}$][c]	112	93	26
CO uptake [$\mu mol\ g^{-1}$][d]	20	21	17
Acid amount [$\mu mol\ g^{-1}$][e]	37	29	17
Density of acid sites [$\mu mol\ m^{-2}$][e]	0.33	0.31	0.65

Estimated by [a]XRD, [a′] TEM, [b]ICP-OES, [c]liquid nitrogen adsorption, [d]CO chemisorption and [e]NH_3-TPD.

2.2. Catalyst characterization methods

Inductively coupled plasma-optical emission spectroscopy (ICP-OES) was performed on the catalyst powder samples, after dissolution in HNO_3/HCl acid, for verification of the Pd and Zn target loadings.

X-ray diffraction (XRD) patterns were obtained with a Siemens Diffractometer 5000 instrument, using Cu Kα radiation. The 2θ angles that were scanned ranged from 10 to 80°. The crystalline bulk phases were identified with the JCPDS reference database.

The surface areas of the samples were determined according to the BET (Brunauer–Emmett–Teller) theory by nitrogen adsorption-desorption isotherms at liquid nitrogen temperature in a Micromeritics ASAP 2010 instrument. Prior to analysis the samples were degassed at 250 °C. Pore size distributions were calculated from the adsorption isotherms by the BJH (Barrett–Joyner–Halenda) model.

CO chemisorption measurements were performed on the powders in a Quantachrome Autosorb-1C system using a volumetric technique. Prior to the measurements, the samples were dried in vacuum at 120 °C, reduced in a flow of H_2 (50 cm^3/min) at 400 °C for 1 h, evacuated at 400 °C for 1 h and then cooled to 35 °C. The CO chemisorption analyses were then carried out using a dual isotherm method.

Temperature-programmed reduction (TPR) and temperature-programmed desorption of ammonia (NH_3-TPD) were conducted using a Micromeritics Autochem 2910 instrument. For the TPR experiments, the reduction was carried out in 5% H_2/Ar at 50 cm^3/min. The samples were first reduced at room temperature by the carrier gas until the hydrogen consumption became negligible. The temperature was thereafter increased up to 600 °C at a heating rate of 10 °C/min. This procedure is described in more detail elsewhere [20]. For the NH_3-TPD experiments, the samples were activated in a flow of He by heating up to 600 °C at 10 °C/min. Catalyst acidity measurements were then started by saturated adsorption of NH_3 at 100 °C followed by flushing with He to remove physisorbed NH_3. TPD was then initiated from 100 °C, at a heating rate of 10 °C/min, up to 600 °C in He.

The composition and morphology of the catalyst samples were studied by transmission electron microscopy (TEM) using a JEM 2000FXII (JEOL) equipped with an energy-dispersive X-ray spectroscopy detector (EDXS) connected to a LINK analyzer system AN 10 000 (Oxford). Images at high resolution were recorded using a transmission electron microscope equipped with a field emission gun, JEM 2100F (JEOL).

2.3. Catalyst activity and selectivity evaluation

The activity and selectivity of the catalysts were evaluated in a stainless steel tubular reactor, mounted vertically and operating at atmospheric pressure. DME, steam and air were fed to the reformer using separate mass flow controllers (Brooks Instruments 5800 series) at an oxygen-to-DME ratio (O_2:DME) of 0.7, a steam-to-DME ratio (H_2O:DME) of 2.5 and a space velocity (GHSV) of 15,000 h^{-1} (NTP). The reactant gases were preheated with a capillary heater and the reactor was heated with a metallic heating coil. The temperature was measured using K-type thermocouples placed at the inlet and outlet of the monolith and at the reactor wall. The experiments were carried out over a temperature interval of 300–450 °C. A porous quartz plate was placed at the reformer inlet to distribute the gases evenly over the cross section of the reactor. The product gas was analyzed with a Maihak Modular System S710 by nondispersive infrared (NDIR) and thermal conductivity (TC) detectors for CO, CO_2 and H_2 and a Gasmet Cr-2000 FTIR instrument for CH_4, CH_3OH, CO, CO_2, DME, HCHO and H_2O. The conversion of oxygen was assumed to be 100%.

The catalysts were evaluated by means of DME conversion and selectivity to hydrogen and carbon dioxide according to Eqs. (1)–(3), where F corresponds to the molar flow rates. $F_{H_2,max}$ is the theoretical maximum hydrogen production at the specific condition, assuming all carbon reacts into CO_2.

$$\text{DME conversion } (\%) = \frac{F_{DME,in} - F_{DME,out}}{F_{DME,in}} \cdot 100 \quad (1)$$

$$H_2 \text{ selectivity } (\%) = \frac{F_{H_2+CO}}{F_{H_2,max}} \cdot 100 \quad (2)$$

$$CO_2 \text{ selectivity } (\%) = \frac{F_{CO_2}}{\sum F_{CO_x}} \cdot 100 \quad (3)$$

3. Results

3.1. Catalyst characterization

3.1.1. X-ray diffraction (XRD)

The crystalline bulk phases of the various samples (after reduction treatment), identified from the X-ray diffraction measurements, are shown in Table 2. As discussed in the introduction section of the paper, PdZn alloys are known to be highly selective in methanol steam reforming, and since methanol is believed to be an intermediate product in DME steam reforming, Pd–Zn interactions are considered essential to achieve high CO_2 selectivity during DME ATR over Pd-based catalysts. The tetragonal PdZn alloy (1:1 atomic ratio) was observed at a 2θ angle of 41.2° and appeared with similar intensity for all samples. No metallic Pd was found, which could be explained by the size of the Pd metal particles being below the detection limit of the instrument. Further, Pd and PdZn peaks may be overlapped by reflections from the supports. Therefore, it was not possible to compare the relative amount of Pd and PdZn present in the samples.

Fig. 1 shows the diffraction patterns between 2θ = 54 and 64°. The diffractogram for the Pd/ZA(1000) sample was found to comprise typical reflections of the spinel-type $ZnAl_2O_4$ phase and ZnO. During impregnation of alumina with zinc nitrate, the surface regions of alumina partly dissolve, and a mixed metal coprecipitate of Zn and Al is formed on the surface [21]. During calcination at high temperature, the regions with Zn–Al then produce $ZnAl_2O_4$, whereas areas with excess of Zn form ZnO. A calcination temperature of 400 °C is not sufficient to form any $ZnAl_2O_4$ phase, hence the Pd/ZA(400) sample consisted mainly of ZnO and γ-Al_2O_3 in addition to the 1:1 PdZn alloy. The Pd/ZA(700) sample was found to consist of a mixture of Al_2O_3 (different transition aluminas), ZnO and $ZnAl_2O_4$ as well as PdZn.

3.1.2. BET surface area, pore size distribution and CO chemisorption measurements

The results from the BET measurements are presented in Table 2. The lowering of the porosity in the support caused by higher calcination temperature resulted in decreasing BET surface areas, from 112 m^2/g for Pd/ZA(400) to 93 m^2/g for Pd/ZA(700) and 26 m^2/g for Pd/ZA(1000). The γ-Al_2O_3 powder used in the physically mixed catalysts had an initial surface area of 150 m^2/g. The pore size distributions of the ZA(400), ZA(700), and ZA(1000) supports are shown in Fig. 2. The amount of pores smaller than 10 nm is found to decrease with the calcination temperature of the support and, concurrently, the fraction of macropores (>50 nm) increases with the calcination temperature. ZA(400) and ZA(700)

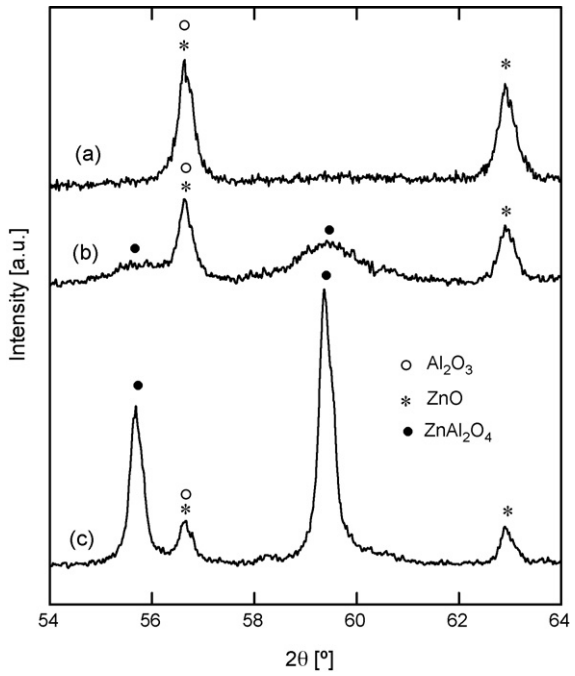

Fig. 1. X-ray diffraction patterns displaying the difference of the supports. (a) Pd/ZA(400), (b) Pd/ZA(700) and (c) Pd/ZA(1000).

are similar, as shown by the XRD results, but the pore volume relative to the surface area is higher for ZA(700) as a result of larger pores created at higher calcination temperature. The maxima in the pore size distribution for the ZA(700) is located at approximately 15 nm, while that for the ZA(400) is closer to 10 nm. The ZA(1000) support exhibited a bimodal pore size distribution with maxima at approximately 15 and 100 nm, respectively.

The ability of Pd to chemisorb CO has been shown to be significantly reduced when Pd is alloyed with Zn [22]. Therefore, CO chemisorption was performed on the catalysts in order to compare the CO uptake of the different samples. The results are presented in Table 2. The CO uptake of the catalysts was found to be similar, despite the differences in BET surface area. The dispersion was estimated assuming an average Pd:CO chemisorption stoichiometry of 1:1 (although the values are likely to be underestimated due to the presence of PdZn). The Pd/ZA(700) sample had the highest dispersion, 6.0%, while the value for Pd/ZA(400) was 5.5% and that for Pd/ZA(1000) 5.3%. The relative error of the measurements was $\leq$7%.

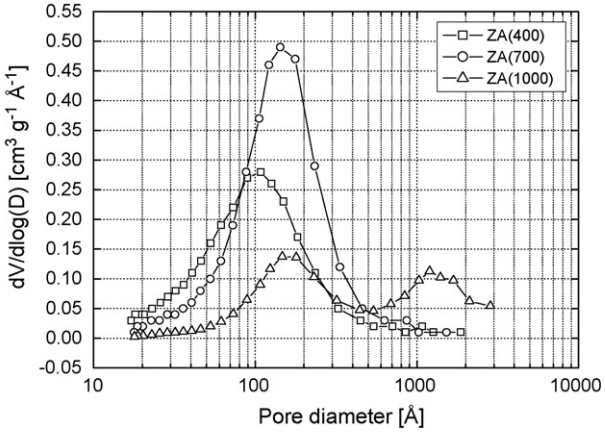

Fig. 2. Pore size distribution of the different supports.

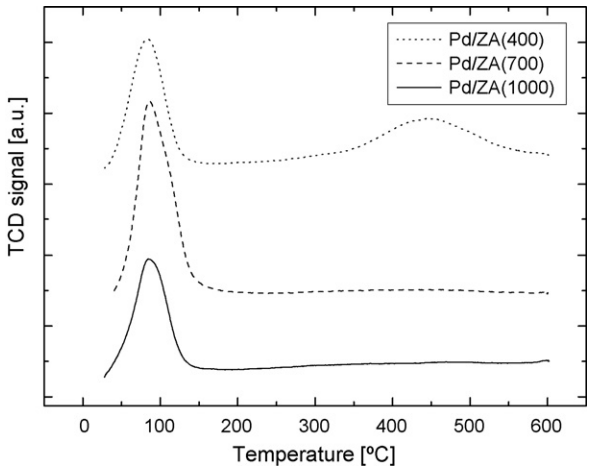

Fig. 3. TPR profiles of the catalyst samples.

3.1.3. Temperature-programmed reduction (TPR)

TPR profiles of the various samples are displayed in Fig. 3. PdO on alumina is normally easily reduced by H_2 at, or even below, room temperature [23]. A fraction of PdO, more strongly bonded to the support, may also be present. In a previous study by the authors, the addition of ZnO to Pd/γ-Al_2O_3 was shown to shift the reduction peaks to lower temperatures during H_2-TPR [18]. Hydrogen consumption was observed at room temperature for all samples but could not be quantified, due to difficulties in obtaining a stable baseline close to room temperature at the beginning of the experiment. A H_2 consumption peak with its maximum at around 90 °C was thereafter observed for all three samples. This peak is ascribed to the formation of metallic Pd and Zn by hydrogen spillover from Pd, as shown by various authors, e.g. Iwasa et al. [24]. The same feature has by the authors been postulated to contribute to high CO_2 selectivity during DME ATR [18]. The Pd/ZA(400) catalyst additionally exhibited a peak at 450 °C. This catalyst contains no $ZnAl_2O_4$ and hence a higher portion of ZnO on the surface of Al_2O_3, why the higher temperature peak may originate from regions of ZnO not being affected by hydrogen spillover from Pd. The TPR profile of ZnO/γ-Al_2O_3, prepared by impregnating alumina with Zn nitrate, exhibits a reduction peak located in this temperature region (not shown in the figure). Alternatively, the higher temperature peak could be due to a fraction of Pd being more strongly bonded to the surface [23]. The H_2 consumption at 90 °C was higher for the Pd/ZA(700) catalyst than for the other samples. This could be due to a higher degree of ZnO reduction into $ZnO_{(1-x)}$ through hydrogen spilt over from Pd or a larger extent of PdZn alloy formation via the subsequent interdiffusion between Pd and $ZnO_{(1-x)}$ [20]. The difference from Pd/ZA(400) is the presence of $ZnAl_2O_4$ which could indicate more loosely bonded PdO. The smaller reduction peak for Pd/ZA(1000) would then be explained by a lower concentration of reducible ZnO.

3.1.4. Temperature-programmed desorption of ammonia (NH_3-TPD)

Temperature-programmed desorption of ammonia was carried out to evaluate the differences in acidity between the materials. The NH_3-TPD profiles are depicted in Fig. 4 and the corresponding amounts of adsorbed NH_3, estimated from the areas underlying the TPD curves, are reported in Table 2. Desorption temperatures indicate the acid strength of the catalysts; stronger acids require higher temperature. Higher acid amount is expected to contribute to higher activity for DME hydrolysis [25]. The spectra in Fig. 4 show significant differences between the various materials. Pd/ZA(400) and Pd/ZA(700) are rather similar, with two distinct peaks

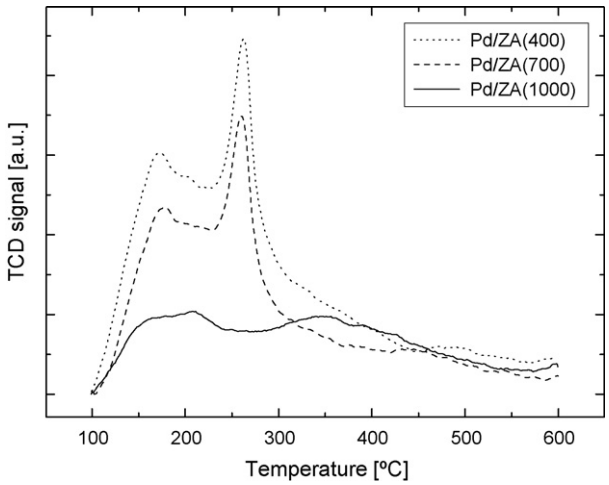

Fig. 4. NH_3-TPD profiles of the catalyst samples.

around 170 °C and 260 °C, although the overall acidity of Pd/ZA(400) is somewhat higher. Pd/ZA(1000) shows no pronounced acidic features and exhibits an overall low acidity. The TPD curve for this catalyst exhibits two broad signals at around 200 °C and 350 °C, followed by a long tail.

3.1.5. Transmission electron microscopy (TEM)

The morphology of the catalyst support material and distribution of palladium in the Pd/ZA(400), Pd/ZA(700) and Pd/ZA(1000) catalysts (after reduction treatment) were investigated by TEM-EDS. The materials were found to be partly inhomogeneous. 50–150 nm sized crystallites of ZnO were observed as agglomerates in some parts of the Pd/ZA(400) catalyst. From EDX measurements and images, the surface of these crystallites was found to be free from palladium and reduced ZnO, see Fig. 5a and b. The main part of the Pd/ZA(400) catalyst support consists of a mixture of γ-Al_2O_3 and ZnO, that overall exhibits a composition close to 2:1 in Al:Zn ratio, equivalent to the stoichiometry of $ZnAl_2O_4$. Dark spots that could be associated to Pd-containing crystals could be observed on this material, with sizes of 3–7 nm, see Fig. 5a and c. A third part of the material in the Pd/ZA(400) catalyst contains excess of Al_2O_3 with about 5–20 at% Zn and 1–5 at% of Pd, see Fig. 5a and d. It was difficult to distinguish the size and shape of the palladium particles or crystallites within this part of the material, which anyhow was quite rare.

The morphology of the support material calcined at 700 °C (ZA(700)) was found to be similar to the ZA(400) material, with the exception that the ZnO–Al_2O_3 material has partly reacted into $ZnAl_2O_4$, thus being more dense. Pd particles were observed on alumina-containing material, but again, not observed on pure ZnO crystals. The distribution of Pd on the $ZnAl_2O_4$ material is shown, by using STEM-HAADF imaging mode, as white dots in Fig. 5e. The corresponding EDX spectra over this fragment give a composition of 5 at% Pd on $ZnAl_2O_4$.

In the Pd/ZA(1000) catalyst, the ZnO crystallites are still observed, while the γ-Al_2O_3 phase has transformed into other alumina phases or reacted with ZnO into $ZnAl_2O_4$. The main part of the Pd/ZA(1000) catalyst is crystalline $ZnAl_2O_4$ supporting facetted particles, see Fig. 5f. By high-resolution imaging of a Pd-containing particle, the observed lattice distances in the Pd-containing crystals could be associated with a PdZn alloy of composition 1:1, see inset in Fig. 5f. To judge whether all Pd are in alloy with Zn or not is almost impossible; likely there is a mixture of Pd, PdZn and Pd_2Zn in the investigated catalysts. However, the main part of the support material changed from mixtures of Al_2O_3 and ZnO in Pd/ZA(400) and Pd/ZA(700), to $ZnAl_2O_4$ in Pd/ZA(1000).

3.2. Catalytic activity and selectivity

In the first part of the monolith catalyst, DME is assumed to react by means of fast oxygen-consuming reactions until all of the oxygen is consumed. Reaction products are CO, CO_2, H_2, and H_2O. The oxidation reactions are used to generate heat to supply the steam reforming reaction in the second part of the monolith, in which the major part of the H_2 is generated. The rate-limiting step during DME steam reforming is DME hydrolysis (Reaction (III) in Table 1) [6]. The conversion of DME into methanol is thermodynamically limited, but when methanol conversion occurs simultaneously, high conversion can be obtained. Efficient catalytic activity for DME hydrolysis is therefore considered essential to reach high conversion of DME by means of the steam reforming reaction. In addition to partial oxidation and steam reforming, a fraction of the DME may be converted via other reaction pathways, such as decomposition reactions (see Table 1). The activity of the Pd-based catalysts during auto-thermal reforming is presented in Fig. 6 as the DME conversion vs. temperature. The conversion was found to increase with the reforming temperature over all of the catalysts. The alumina-mixed catalysts were more active than the corresponding single catalysts. At a reforming temperature of 400–450 °C, the order of activity was as follows: Pd/ZA(1000)+γ-Al_2O_3 > Pd/ZA(1000) >Pd/ZA(700) + γ-Al_2O_3 > Pd/ZA(400) >Pd/ZA(700). The Pd/ZA(1000) + γ-Al_2O_3 catalyst, was significantly more active than the other catalysts over the entire temperature range studied and reached a conversion close to 100% at 450 °C. The Pd/ZA(1000) catalyst exhibited much lower activity up to a temperature of 400 °C, when it after a sharp increase (see Fig. 6), starting at 350 °C, approached the Pd/ZA(1000) + γ-Al_2O_3 catalyst.

The hydrogen selectivity for the various catalysts, at 300–450 °C, is shown in Fig. 7. Increasing temperature resulted in higher H_2 selectivity, as a result of the increase in DME conversion. The H_2 selectivity was significantly higher for the alumina-mixed catalysts than for the single catalysts. Both Pd/ZA(700) + γ-Al_2O_3 and Pd/ZA(1000) + γ-Al_2O_3 approached 100% selectivity to hydrogen at 450 °C. However, the difference in H_2 selectivity between the catalysts did not follow the same order as the conversion, suggesting differences between the catalyst materials that influence the selectivity to hydrogen. Pd/ZA(1000) exhibited lower selectivity to hydrogen despite having the second highest activity, indicating lower steam reforming activity over this catalyst.

Fig. 8 shows the selectivity to CO_2 at reforming temperatures between 300 and 450 °C for the DME ATR catalysts. For physical mixtures of the catalysts with alumina, the CO_2 selectivity was found to increase over the temperature range, whereas slight decreases in selectivity were observed for the single catalysts. Increases in CO_2 selectivity with increasing temperature may result from a higher extent of total oxidation or steam reforming of DME. An observed increase of H_2 and CO_2, accompanied by a decrease in the water concentration, indicates that the steam reforming activity increases at higher temperature for the alumina mixtures. However, the alumina mixtures exhibited an overall lower selectivity to CO_2. The Pd/ZA(400) and the Pd/ZA(700) catalysts were considerably more selective than the Pd/ZA(1000) catalyst. At 400 °C, where the conversion of the Pd/ZA(1000) catalyst approached that of its alumina-mixed counterpart (Fig. 6), the CO_2 selectivity of this catalyst decreased to a value below those of the physically mixed catalysts. At 450 °C, the order of CO_2 selectivity was the following: Pd/ZA(700) ~Pd/ZA(400) > Pd/ZA(700) + γ-Al_2O_3 > Pd/ZA(1000) + γ-Al_2O_3 > Pd/ZA(1000).

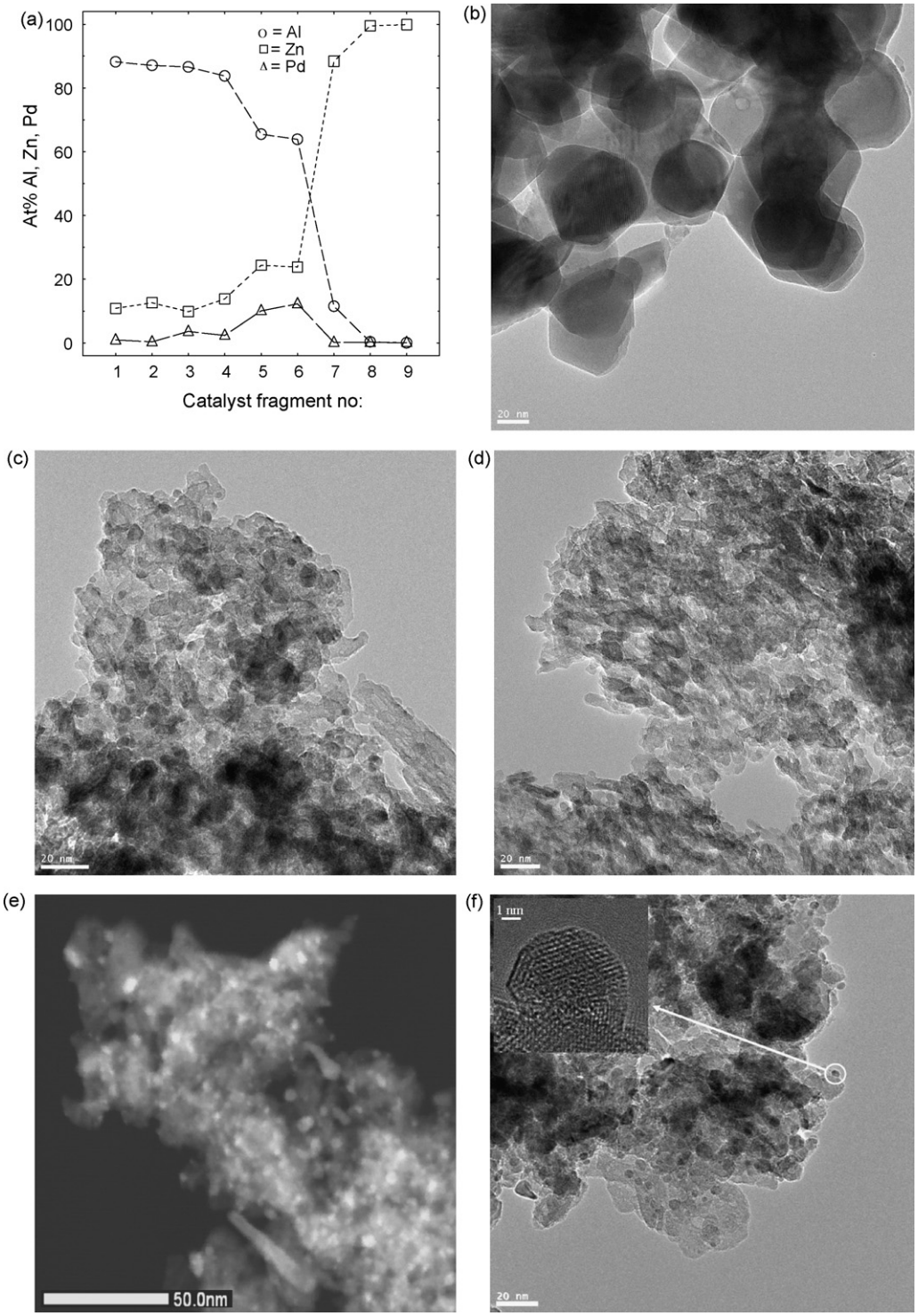

Fig. 5. Plot of EDX data obtained from nine fragments of the Pd/ZA(400) catalyst (a) and corresponding TEM images of fragment No. 9 (b), No. 6 (c) and No. 4 (d). Distribution of Pd particles in a fragment with 5 at% Pd and a Zn:Al ratio of 1:2 in the Pd/ZA(700) catalyst, imaged in STEM-HAADF mode as white dots (e). The corresponding material in the Pd/ZA(1000) catalyst is shown in (f), with an inset of a PdZn particle anchored on the support material. All samples were reduced at 400 °C in 1000 Ncm^3/min flow of 5% H_2/N_2 for 1 h.

The concentrations of CH_4, CO, and CH_3OH in the product gas at 450 °C using the different catalysts are shown in Fig. 9. Pd/ZA(400), Pd/ZA(700), and Pd/ZA(1000) were found to generate methane concentrations ranging from 1.7 to 2.1 mol%. The methane is likely to originate from the direct decomposition of DME into CH_4, CO, and H_2 (Reaction (VI) in Table 1). Decomposition of DME occurs via methyl (CH_3) and methoxy (CH_3O) species [26] and the methyl can easily be further hydrogenated to form methane. The methane concentration was found to increase with the temperature. The CH_4:CO ratios for Pd/ZA(400) and Pd/ZA(700) were close to 1 at 450 °C, which implies that all of the CO is generated through decomposition of DME over those catalysts. The alumina mixtures generated methane concentrations below 4000 ppm. This feature, together with small amounts of methanol observed in the product

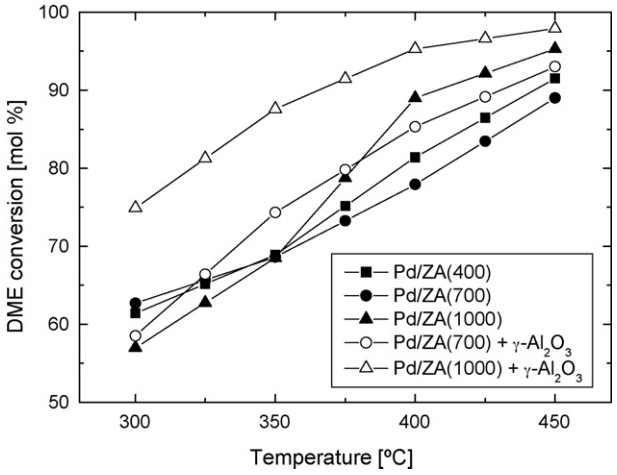

Fig. 6. Activity of the catalysts for autothermal reforming of DME (Reaction conditions: O_2:DME = 0.7, H_2O:DME = 2.5 and GHSV = 15000 h^{-1}).

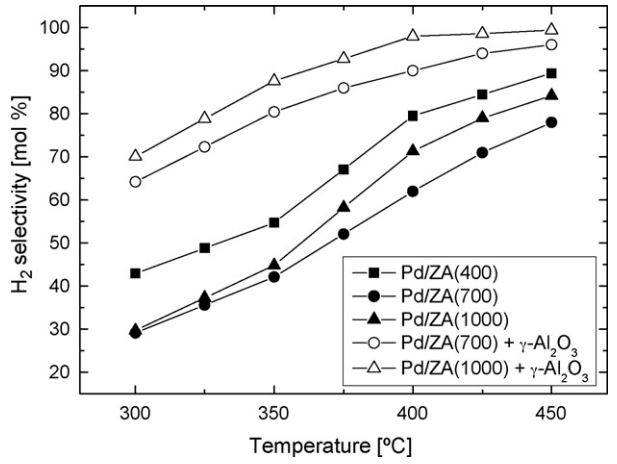

Fig. 7. H_2 selectivity during autothermal reforming over the various catalysts (Reaction conditions: O_2:DME = 0.7, H_2O:DME = 2.5 and GHSV = 15000 h^{-1}).

gas during reforming of the alumina mixtures, indicates that the CO originates from decomposition of methanol formed by hydrolysis over alumina. Methanol was also observed during reforming over the Pd/ZA(1000) catalyst, and methanol decomposition may explain the higher concentration of CO for this catalyst compared to the Pd/ZA(400) and Pd/ZA(700) catalysts. Nevertheless, high selectivity to hydrogen and carbon dioxide was observed for all catalysts and indicates high activity for autothermal reforming of DME.

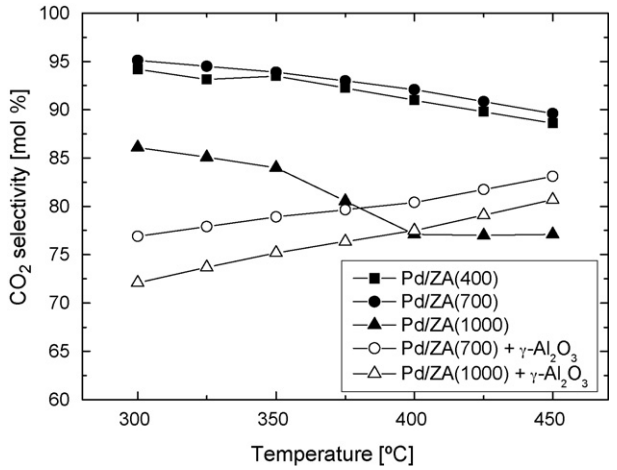

Fig. 8. CO_2 selectivity during autothermal reforming of DME over the various catalysts (Reaction conditions: O_2:DME = 0.7, H_2O:DME = 2.5 and GHSV = 15000 h^{-1}).

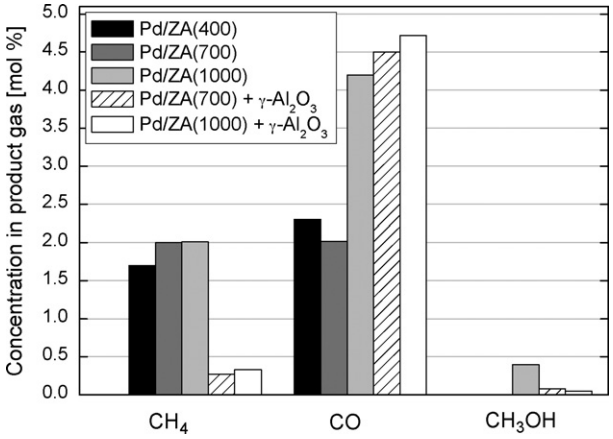

Fig. 9. Concentration of CH_4, CO, and CH_3OH in the product gas during autothermal reforming of DME at 450 °C (Reaction conditions: O_2:DME = 0.7, H_2O:DME = 2.5 and GHSV = 15000 h^{-1}).

4. Discussion

Three different catalyst materials, with the same amounts of Pd, Zn and Al, but with varying chemical composition, acidity, and textural properties, have been evaluated for dimethyl ether autothermal reforming. The aim was to obtain interactions between Pd and Zn, supposed to be responsible for high CO_2 selectivity, and at the same time having sites available for hydrolysis of DME. Therefore, the approach was to prepare materials consisting of mixtures of phases that could result in a catalyst with a suitable combination of properties in order to achieve activity for all desired reactions. As mentioned in the introduction, the presence of $ZnAl_2O_4$ and ZnO is believed to be able to prevent interactions between Pd and Al_2O_3 and subsequently to avoid the formation of Pd^0/Al_2O_3 sites, in accordance with the results from Liu et al. [19]. During autothermal reforming conditions, several reactions may be competing on the catalyst surface. The desired reactions are DME steam reforming, DME partial oxidation and water-gas shift, whereas decomposition reactions, that generate higher concentrations of CO, are unwanted. As some of the reactions involved during DME ATR occur simultaneously, separate catalyst beds or segments, active for individual reactions, cannot be used. Complex catalyst materials in addition to the complex reaction network pose difficulties to entirely interpret phenomena during reaction. Catalyst properties may be interrelated and it can therefore be difficult to distinguish which effects are the most relevant as several properties can be responsible for a specific characteristic. Some of the aspects involved during DME ATR are considered and discussed in the following, based on the results from the activity tests and characterization studies.

4.1. Activity and selectivity of the DME ATR catalysts

The results presented in this study suggest that the activity of PdZn-based catalysts for DME ATR can be enhanced by tuning of the support. Pd supported on Zn–Al mixed oxides exhibited higher activity compared to a γ-Al_2O_3-supported catalyst. Although acidity seems to be important for the catalytic activity, the

differences in total acid amount between the catalysts, as shown by NH_3-TPD measurements (Table 2), cannot be directly related to the ability of the catalysts to convert DME. At higher calcination temperature of the support, less acidic transition aluminas and zinc aluminate are formed. Furthermore, the NH_3-TPD results are reflections of the BET surface areas. Pd/ZA(400) and Pd/ZA(700) are similar, in accordance with the XRD results. The Pd/ZA(1000) catalyst had the lowest total acid amount of the catalysts but was the most efficient in converting DME. On the other hand, because the surface area is lower for the Pd/ZA(1000) catalyst, the density of acid sites is higher for this catalyst (see Table 2), which may influence the catalytic activity by creating closer intimacy between the different types of sites. The dispersion of Pd was found to be similar for the three catalysts and, therefore, this feature could not be used to explain the difference in activity. As previously mentioned, the CO chemisorption ability of Pd could be affected in the presence of strong Pd–Zn interactions. It is therefore difficult to conclude if the similar CO uptakes for the catalysts (20, 21, and 17 μmol/g catalyst, respectively) are in fact due to comparable dispersion or if there are also differences considering the extent of PdZn alloy formation. As a result of the decreased surface area at higher calcination temperature, a logical effect would be decreased metal dispersion. The similar CO uptakes, despite differing BET surface areas, for the three samples may possibly be explained by a higher extent of PdZn formation in the Pd/ZA(400) and Pd/ZA(700) catalysts, which then could be correlated to the higher CO_2 selectivity for those catalysts. In the TEM analyses, the Pd/ZA(400) and Pd/ZA(700) catalysts were found to contain areas consisting of excess ZnO without any Pd particles on the surface. However, in the main part of the catalysts, the Pd-containing particles appeared well dispersed, with similar particle sizes as in the Pd/ZA(1000) catalyst. The particle sizes can also be estimated from the chemisorption results by taking the reciprocal of the measured metal dispersion [27,28]. Since the obtained values are far from the particle sizes observed during TEM (3–7 nm), it is reasonable to assume that the CO uptake has been affected by the formation of PdZn alloys and that the dispersion in fact is higher.

The higher activity of the Pd/ZA(1000) catalyst may to some extent be related to the difference in pore size distribution of the support. This catalyst exhibited a bimodal pore size distribution, as shown in Fig. 2. It can be expected that larger pores and lower porosity lead to more rapid transportation of reactants to the active sites. The hydrophobic nature of $ZnAl_2O_4$, in contrast to Al_2O_3, may also be correlated with the differing activities due to changes in the rate of H_2O adsorption, although this effect was not investigated in the present study. Hydrophobic/hydrophilic features have previously been postulated to influence hydrolysis activity during DME steam reforming [6,7]. While the accessibility of the active sites is essential, higher acidity then contributes to higher activity for the DME hydrolysis reaction. Physical mixing of the catalysts with alumina resulted in higher conversion, indicating the importance of acid sites. The lower amount of acid sites for the Pd/ZA(1000) catalyst compared to the other catalysts could be the reason for the higher temperatures needed for conversion over this catalyst, when not mixed with γ-Al_2O_3. During partial oxidation of DME, less acidic oxides have been shown to shift the active temperature range to higher temperatures [10]. On the other hand, more acidic supports, such as alumina, have been shown to cause severe coke deposition both during partial oxidation [10] and steam reforming [25] of DME. Inspection of the catalysts after the experiments revealed only small amounts of coke, concentrated at the inlet of the catalysts, but the amount was not quantitatively determined. More coke was, however, observed on the alumina mixtures than on the non-mixed catalysts. As catalyst durability is a key factor for practical use, long-term stability tests are needed to investigate if the coking will result in deactivation over time.

Pd–Zn alloy formation following reduction at 400 °C was confirmed by TEM, TPR, and XRD. The CO_2 selectivity was higher for the single catalysts compared to their corresponding alumina mixtures. It is believed that monometallic Pd on alumina is the explanation to the lower CO_2 selectivity in the alumina mixtures, but this could not be verified by ex-situ characterization techniques. Karim et al. [14] have shown that, during methanol steam reforming, it is the small monometallic Pd particles that are detrimental to the overall CO_2 selectivity, irrespective of the extent of PdZn alloy formation. In the present study, the catalysts exhibited high selectivity to CO_2 even though a substantial amount of small Pd particles were observed during the TEM analyses.

The single catalysts (Pd/ZA(400), Pd/ZA(700), and Pd/ZA(1000)) generated higher concentrations of methane than the catalysts mixed with alumina. This methane is supposed to be formed through decomposition reactions. CO methanation was not considered important, as Pd catalysts, in the presence of water, promote the water-gas shift reaction resulting in poor methanation activity [29]. Methane is inert in the fuel cell reactions; hence the methane remaining after the reformer will eventually end up in an afterburner. However, the methane occupies hydrogen and, therefore, it is desirable to decrease the methane concentration in order to further increase the hydrogen yield. Methanol was observed in the product gas during reforming over the alumina mixtures and over the Pd/ZA(1000) catalyst. For the Pd/ZA(1000) catalyst, the concentration of methanol increased with temperature up to 400 °C, which indicates that the methanol steam reforming is rate limiting for this catalyst. The absence of methanol in the product gas during reforming of Pd/ZA(400) and Pd/ZA(700) implies that the rate of methanol consumption is higher than the DME hydrolysis rate over those catalysts.

4.2. Additional remarks

It appears, as if different properties are responsible for activity and selectivity, respectively. The support seems to play a key role for the performance of the catalysts. The catalyst should be designed to contain the adequate combination of properties, which are known to result in high activity and selectivity. The optimal DME ATR catalyst will be one where Pd is in close contact with Zn and the reaction occurs via methanol and avoids the formation of methane through decomposition. The activity is believed to be influenced by the accessibility of the active sites for the reactants as well as the acidity of the support. Possible factors affecting the accessibility for the reactants in the evaluated catalysts may include hydrophobicity/hydrophilicity and pore size distribution of the support. Improved activity of PdZn-based catalysts for the desired reactions is suggested to be possible by (1) tuning the support for maximum access to the active sites, (2) increasing the density of acid sites for enhanced intimacy with Pd, and (3) ensuring the Pd particles are strongly anchored to Zn. Evaluation of catalyst preparation parameters including thermal treatments (calcination and reduction) will be the subject of future studies. The PdZn alloy is formed during pretreatment of the catalysts, but hydrogen generated during reforming could facilitate the formation. Further, the influence of hydrophobicity and pore size of the support need to be evaluated.

The DME ATR catalysts evaluated in this study are aimed for automotive applications, with high demands on mechanical stability and low pressure drop. Therefore, the activity tests of

the catalysts were performed using monolith substrates. The drawback with monoliths, however, is that a lower amount of active material can be deposited per volume of catalyst than for fixed bed catalysts. Nevertheless, considering the difference in residence time compared to other studies in the literature where fixed bed reactors are used, the results in this study appear very promising. In a fuel cell fuel processor, the DME-fuelled reformer could be coupled with a water-gas shift unit, where the CO concentration can be reduced to approximately 0.5–1%. The product gas from the water-gas shift reactor could be used to feed high-temperature polymer electrolyte fuel cells without further cleanup. In other words, the complexity of the overall fuel processing system will be significantly lower running on DME compared to a diesel or gasoline-fueled APU, which requires a number of cleanup steps (of both CO and sulfur) and consequently also a more complex heat management.

5. Conclusions

Impregnation of Pd onto mixtures of ZnO, $ZnAl_2O_4$, and Al_2O_3, followed by reduction treatment, results in catalyst materials with high activity for the reactions involved during autothermal reforming of dimethyl ether. The Zn–Al mixed oxides, generated by thermal treatment of a binary $ZnO–Al_2O_3$ support, exhibited improved activity compared to a γ-Al_2O_3-supported PdZn catalyst. No decline in activity was observed despite decreasing surface areas (from 112 to 26 m^2/g) and decreasing number of acid sites, resulting from higher calcination temperature of the support. The highest conversion of DME was obtained for the Pd/ZA(1000) catalyst (S_A = 26 m^2/g), in which the support comprises mainly the $ZnAl_2O_4$ phase.

Physical mixing of the catalysts with γ-Al_2O_3 resulted in increased conversion but a decrease in the CO_2 selectivity. The order of activity in the temperature range of 400–450 °C for the catalysts tested was the following: Pd/ZA(1000) + γ-Al_2O_3 > Pd/ZA(1000) >Pd/ZA(700) + γ-Al_2O_3 > Pd/ZA(400) >Pd/ZA(700). The Pd/ZA(1000) + γ-Al_2O_3 catalyst converted almost 100% of the DME with hydrogen selectivity close to 100% at 450 °C.

CO_2, CO and CH_4 were the primary carbon-containing products and CH_3OH were found in small amounts for some catalysts. The CO_2 selectivity was high and was correlated with the presence of a PdZn phase. CO concentrations below 5% were obtained for all catalysts. The reformate from a DME-fuelled autothermal reformer could therefore be coupled with a water-gas shift unit to achieve CO concentrations of 0.5–1%. Thus, the overall fuel processor system will be of low complexity, which is advantageous in automotive applications such as fuel cell auxiliary power units. The CO generated is suggested to originate primarily from decomposition of methanol and dimethyl ether.

Acknowledgements

The Swedish Energy Agency, the Swedish Agency for Innovation Systems, the Swedish Road Administration and the Swedish Environmental Protection Agency are gratefully acknowledged for financial support to this work. Thanks also to Corning Inc. for supplying cordierite substrate and to Sasol Germany GmbH for providing alumina. The Knut and Alice Wallenberg Foundation is acknowledged for financial support to the new EM facilities installed at FOOS, Stockholm University.

References

[1] CONCAWE, EUCAR, JRC, Well-to-wheels analysis of future automotive fuels and powertrains in the European context, Well-to-Wheels Report, Version 2c, March 2007.
[2] J. Zhang, Z. Xie, J. Zhang, Y. Tang, C. Song, T. Navessin, Z. Chi, D. Song, H. Wang, D.P. Wilkinson, Z.-S. Liu, S. Holdcroft, J. Power Sources 160 (2006) 877–891.
[3] V. Galvita, G. Semin, V. Belyaev, T. Yurieva, V. Sobyanin, Appl. Catal. A 216 (2001) 85–90.
[4] T. Matsumoto, T. Nishiguchi, H. Kanai, K. Utani, Y. Matsumura, S. Imamura, Appl. Catal. A 276 (2004) 267–273.
[5] K. Takeishi, H. Suzuki, Appl. Catal. A 260 (2004) 111–117.
[6] T.A. Semelsberger, K.C. Ott, R.L. Borup, H.L. Greene, Appl. Catal B 61 (2005) 281–287.
[7] K. Faungnawakij, Y. Tanaka, N. Shimoda, T. Fukunuga, S. Kawashima, R. Kikuchi, K. Eguchi, Appl. Catal. A 304 (2006) 40–48.
[8] J. Agrell, B. Lindström, L.J. Pettersson, S.G. Järås, in: J.J. Spivey (Ed.), Catalysis—Specialist Periodical Reports, 16, Royal Society of Chemistry, Cambridge, 2002 pp. 67–132.
[9] Q. Zhang, X. Li, K. Fujimoto, K. Asami, Appl. Catal. A 288 (2005) 169–174.
[10] S. Wang, T. Ishihara, Y. Takita, Appl. Catal. A 228 (2002) 167–176.
[11] M. Flytzani-Stephanopoulos, G.E. Voecks, U.S. DOE Report DOE/ET-11326–1, 1980.
[12] B. Lindström, L.J. Pettersson, Catal. Lett. 74 (2001) 27–30.
[13] N. Iwasa, T. Mayanagi, W. Nomura, M. Arai, N. Takezawa, Appl. Catal. A 248 (2003) 153–160.
[14] A. Karim, T. Conant, A. Datye, J. Catal. 243 (2006) 420–427.
[15] Y. Usami, K. Kagawa, M. Kawazoe, Y. Matsumura, H. Sakurai, M. Haruta, Appl. Catal. A 171 (1998) 123–130.
[16] Y. Matsumura, M. Okumura, Y. Usami, K. Kagawa, H. Yamashita, M. Anpo, M. Haruta, Catal. Lett. 44 (1997) 189–191.
[17] Z.X. Chen, K.M. Neyman, A.B. Gordienko, N. Rösch, Phys. Rev. B 68 (2003) 075417.
[18] M. Nilsson, P. Jozsa, L.J. Pettersson, Appl. Catal. B 76 (2007) 41–49.
[19] S. Liu, K. Takahashi, H. Eguchi, K. Uematsu, Catal. Today 129 (2007) 287–292.
[20] C. Hong, C. Yeh, F. Yu, Appl. Catal. 48 (1989) 385–396.
[21] T. Trainor, G.E. Brown Jr., G.A. Parks, J. Colloid Interface Sci. 231 (2000) 359–372.
[22] J.A. Rodriguez, J. Phys Chem. 98 (1994) 5758–5764.
[23] H. Lieske, J. Völter, J. Phys. Chem. 89 (1985) 1841–1842.
[24] N. Iwasa, N. Ogawa, S. Masuda, N. Takezawa, Bull. Chem. Soc. Jpn. 71 (1998) 1451–1455.
[25] K. Faungnawakij, R. Kikuchi, T. Matsui, T. Fukunaga, K. Eguchi, Appl. Catal. A 333 (2007) 114–121.
[26] L. Bugyi, F. Solymosi, Surf. Sci. 385 (1997) 365–375.
[27] G. Bergeret, P. Gallezot, in: G. Ertl, H. Knözinger, J. Weitkamp (Eds.), Handbook of Heterogeneous Catalysis, VCH, Weinheim, 1997, pp. 439–464.
[28] M. Boudart, G. Djéga-Mariadassou, Kinetics of Heterogeneous Catalytic Reactions, Princeton University Press, Princeton, 1984, 20–26.
[29] P. Panagiotopoulou, D. Kondarides, X.E. Verykios, Appl. Catal. A: Gen. 344 (2008) 45–54.